This document is the accepted manuscript version of the following article:
Wüest, R. O., Bergamini, A., Bollmann, K., & Baltensweiler, A. (2020). LiDAR data as a proxy for light availability improve distribution modelling of woody species. Forest Ecology and Management, 456, 117644 (10 pp.). https://doi.org/10.1016/j.foreco.2019.117644

This manuscript version is made available under the CC-BY-NC-ND 4.0 license http://creativecommons.org/licenses/by-nc-nd/4.0/

LiDAR data as a proxy for light availability improve distribution modelling of woody species

Authors

Rafael O Wüest[a,*], Ariel Bergamini[a], Kurt Bollmann[a], Andri Baltensweiler[a]

[a] Swiss Federal Institute for Forest, Snow and Landscape Research WSL, Zürcherstrasse 111, CH-8903 Birmensdorf, Switzerland

[*] corresponding author; rafael.wueest@gmail.com; Swiss Federal Institute for Forest, Snow and Landscape Research WSL, Zürcherstrasse 111, CH-8903 Birmensdorf, Switzerland

Declarations of interest

Declarations of interest: none

Abstract

Modern multifunctional forest management can profit from high-quality information on the potential distribution of woody species generated by species distribution models (SDMs). Forest structure is an important factor in determining the distribution of woody species in forests, for example because it affects light conditions within forest stands. Remotely sensed data from light detection and ranging (LiDAR) can capture this three-dimensional structure of forests, leading to the expectation that LiDAR-derived data should enhance the predictive performance of SDMs. We test if and how LiDAR-derived data increases the predictive performance of SDMs for light-demanding and shade-tolerant shrub and tree species in Swiss Forests. Our analyses suggest that LiDAR-derived data generally increases predictive performance of models. However, the response to including LiDAR-derived data varies depending on plant functional type: the increase in predictive performance is largest for light-demanding shrubs, reduced for light-demanding trees, and is lost for shade-tolerant species. We further find that shade-tolerant and light-demanding species show opposing responses along the LiDAR-derived predictors. Our results suggest that LiDAR-derived data indeed capture some aspects of light availability in forests, and that including LiDAR-derived predictors in SDMs should be considered for light-demanding shrubs, but may be of less use for trees (especially if shade-tolerant). We conclude that improving SDMs and resulting maps by including LiDAR-derived predictors potentially helps to ameliorate multifunctional, biodiversity-friendly forest stand management.

Keywords

LiDAR; airborne laser scanning; forest structure; habitat suitability models; distribution map; light availability

1 Introduction

The growing engagement for multifunctional, biodiversity-friendly forest management (Gustafsson et al., 2012; Lindenmayer and Franklin, 2002), has spurred the interest in modeling the potential distribution of forest species using so-called species distribution models (Guisan and Thuiller, 2005; SDMs, Guisan and Zimmermann, 2000). The quality and usefulness of SDMs for forest species depends on developing accurate and precise predictors for climatic conditions (e.g., temperature), local resource availability (e.g., soil characteristics) and structural forest features (e.g., crown heterogeneity). In recent years, airborne light detection and ranging (LiDAR) data became increasingly available and have proven to be important predictors in biodiversity modeling. For example, LiDAR data enhance species richness predictions (Bouvier et al., 2017; Camathias et al., 2013; Clawges et al., 2008; Simonson et al., 2014; Zellweger et al., 2016), improve predicting community composition and changes (Thers et al., 2017; Zellweger et al., 2017), help explaining animal distribution and behavior (Ciuti et al., 2018; Davies et al., 2017; Froidevaux et al., 2016), and increase the quality of SDMs for birds (Farrell et al., 2013; Vierling et al., 2013; Zellweger et al., 2013).

The main factor that makes LiDAR data informative in biodiversity modeling is their capacity to describe the 3D structure of vegetation, particularly in forests (Lefsky et al., 2002). Forest structure, in turn, is known to be a key determinant of the distribution of woody plant species in forests because it affects both the quantity and heterogeneity of light, a key resource for woody species growing in forests (Bartels and Chen, 2010; Kumar et al., 2010). Forest disturbance, natural or induced by management, affects light availability, diversity and composition of understory tree and shrub species in the short and long term (Ares et al., 2010; e.g., Halpern et al., 2012; Taki et al., 2010). In the absence of management or disturbance, mortality-induced changes in the abundance patterns of canopy species change

64 the canopy structure and its light transmittance, which affects the composition of subcanopy
65 communities (reviewed in Barbier et al., 2008). Despite these demonstrated effects of forest
66 structure on the distribution of woody species, and in contrast to animal ecology (Davies and
67 Asner, 2014), quantitative vegetation structural attributes based on LiDAR data have rarely
68 been used in species distribution models for woody species.
69 The use of LiDAR data in SDMs for woody species can be problematic because woody
70 species are not only affected by vegetation structure, they also define it to a large degree. In
71 other words, woody species define the 3D structure of forests habitats, but this structure also
72 defines how suitable that habitat is for woody species. Although this circularity is routinely
73 used when attempting to map the actual distribution of woody species (Alonzo et al., 2014;
74 Brandtberg, 2007; e.g. Holmgren and Persson, 2004; Shi et al., 2018), it can lead to the
75 underestimation of suitable habitat when spatially projecting the potential distribution of
76 woody species using SDMs (Bradley et al., 2012). Essentially, this could mean that managers
77 take wrong decisions because of erroneous predictions from SDMs (for example, because
78 potentially suitable habitat is not recognized). In an attempt to develop guidance on when and
79 how to include LiDAR data in SDMs of woody species, we propose to define ecologically
80 based hypotheses on how the use of LiDAR data should affect the predictive performance of
81 SDMs for different functional groups (light-demanding vs. shade-tolerant shrubs and trees),
82 and how these functional groups respond along pivotal LiDAR gradients.
83 The goal of this study is to reveal the usefulness and appropriateness of including LiDAR
84 data in SDMs for woody species. We used the extensive data of the Swiss National Forest
85 Inventory (Brassel and Lischke, 2001) for testing four hypotheses (Table 1). The fact that
86 forest structure is important in determining habitat and light conditions in forests leads to the
87 hypothesis H1 that LiDAR data should generally increase the predictive performance of
88 SDMs for woody species. The second hypothesis H2 relates to the growth-form of woody

species. Whereas tall-growing trees can reach the canopy at some point and thus are exposed to direct sunlight, the smaller shrubs will never reach the canopy. Hence, we expect that the increase of predictive performance is greater in SDMs for shrubs than for trees. The third hypothesis H3 is associated with the light requirements of woody species. Shade-tolerant species, as indicated by their name, can tolerate shade, which implies that they also can grow in conditions with more available light. This is not true for light-demanding species: they demand a minimum of available light. Therefore, we expect that the positive effect of LiDAR data on the predictive performance of SDMs should be greater in light-demanding species than in shade-tolerant species. The fourth hypothesis H4 predicts opposing responses along LiDAR gradients for woody species with differing light requirements. We hypothesize that light-demanding species should positively relate to LiDAR data that characterize open, sparsely vegetated forest stands, while shade-tolerant species should relate positively to LiDAR data that captures shading through (dense) vegetation. We tested the four hypotheses by assessing the predictive performance of a set of SDMs without LiDAR data (based solely on climatic, topographic and soil predictors) and with LiDAR data for a total of eight species, by choosing two woody species from each of the four functional groups (shade-tolerant and light-demanding shrubs and trees).

Table 1 The four hypotheses H1 to H4 that are tested in this study are in the first column, with a prediction on what we expect to find in the statistical analyses in the second column (for details on the statistical analyses see section 2.4.1).

	Hypothesis	**Prediction**
H1	LiDAR data should generally increase the predictive performance of SDMs	higher intercept for models that include LiDAR data
H2	increase of predictive performance when including LiDAR data is greater in SDMs for shrubs than for trees	negative interaction effect for trees
H3	increase of predictive performance when including LiDAR data is greater in SDMs for light-demanding species than for shade-tolerant species	negative interaction effect for shade-tolerant species
H4	shade-tolerant and light-demanding species should show opposing responses along LiDAR gradients	details see Figure 1 and section 2.2.3

2 Methods

2.1 Study area and species data

Our study area is Switzerland, covering an area of ca. 41'000 km2 in Europe (45,82° to 47,81° N, 5,96° to 10,5° E). Approximately one third of the country is covered by forests, and 99% of these forests are distributed between 330 and 2140 m a.s.l. We used presence-absence data of woody species from the fourth National Forest Inventory (NFI4, 2009 to 1017). The Swiss NFI collects data of 138 woody species across a regular grid with 1.4 km resolution

(Keller, 2011). At each forested grid-location (N= 6352), the NFI records the presence of all woody species with heights taller than 40 cm in a circular area of 200 m^2 (7.98 m radius). In a larger circle of 500 m^2 (12.62 m radius), all trees with a diameter at breast height larger than 36 cm are recorded. In accordance with Zurell et al.(2019), all species that were not recorded as present were assumed to be absent.

Our hypotheses (see Table 1) relate to four distinct functional groups of woody species (light-demanding vs. shade-tolerant shrubs and trees). Therefore, we used information from the Flora Indicativa (Landolt et al., 2010) in order to characterize all species regarding their light requirements and life form. We classified all species from the Swiss NFI that were listed in the Flora Indicativa as phanerophyte and grow taller than 4 meters as tree species. We used the "light indicator value" that describes the species' light requirements using five classes that range from one (deep shade) to five (full light): we classified all species with indicator values 1-2 (deep shade, shade) as shade-tolerant and those with values 4-5 (well-lit, full light) as light-demanding. An indicator value of 3 indicates medium light conditions and was therefore not added to either class. The resulting list contained 24 candidate species (see Table A1 in the supplementary information) from which two species for each of the four functional classes were selected. We considered the number of observations in the Swiss NFI as selection criteria as well as the economic importance (in the case of tree species), while simultaneously aiming for a broad taxonomic coverage. The selected set of species included *Juniperus communis* and *Prunus spinosa* (light-demanding shrubs), *Daphne mezereum* and *Lonicera nigra* (shade-tolerant shrubs), *Populus termula* and *Pinus sylvestris* (light-demanding trees), *Fagus sylvatica* and *Picea abies* (shade-tolerant trees; see Table A1 for a tabular listing of the selected species).

2.2 Environmental data

2.2.1 Climate, topography, soils

We compiled a set of 17 climatic and 40 topographic predictors as well as one soil predictor at a resolution of 25 m, which corresponds well with the species data of the reference area in the NFI (a circle with a diameter of 25.24 m). The climatic predictors were based on monthly temperature, precipitation, and potential evapotranspiration layers from Zimmermann and Kienast (1999). The topographic predictors were based on a 25 m digital elevation model for Switzerland (Swisstopo, 2010a) in order to reflect the topography of the surrounding landscape, and were calculated using the SAGA GIS v. 2.1.2 (Baltensweiler et al., 2017; Conrad et al., 2015). We also used a 5 m digital elevation model to describe microtopographic variation within a cell of the target resolution (Swisstopo, 2010b). The soil predictor consisted of a modeled pH layer that was based on >1500 soil profiles in Swiss forests. Please see Table A2 for the details of these climatic, topographic and soil predictors which were selected while building the SDMs.

2.2.2 LiDAR-derived predictors

We derived vegetation structural indicators (average vegetation height, vegetation cover, foliage height diversity, and vertical coefficient of variation) at the same resolution (25 m) from a nation-wide LiDAR dataset, provided by the Swiss Federal Office of Topography (Swisstopo, 2010b), updated with various cantonal LiDAR datasets. The Swisstopo LiDAR dataset was acquired during multiple seasons between 2000 and 2007 with a minimal point density of 0.5 m^{-2} (Artuso et al., 2003). The data acquisitions of cantonal datasets occurred in the years 2005 to 2014 with a return density between 4 to 15 points/m^2. Subsampling areas of higher point densities to the lower densities showed that the variation in density did not affect the pixel specific values of the structural variables at the resolution of 25 meters (in agreement with Wilkes et al., 2015; Table A3).

As LiDAR data was only available for areas below ca. 2000 m a.s.l, we had to remove NFI-observations without LiDAR data, leading to a total N = 5551 observations.

Using the LAStools software (Isenburg, 2015), we developed four LiDAR-derived predictors (average vegetation height, vegetation cover, foliage height diversity, and vertical coefficient of variation) to describe forest structure. To normalize the LiDAR return heights we used the SwissALTI3D digital terrain model that has a horizontal resolution of 2 m by 2 m and is based on the Swisstopo LiDAR dataset and reaches ± 0.5 m accuracy (one standard deviation) in all three dimensions (Swisstopo, 2010b). Average vegetation height was calculated as the mean height of all points between 0.4 and 55.0 m. We chose the lower limit to align with the minimal size that plants had to reach in order to be recorded in the Swiss NFI (40 cm), and the upper limit of 55 m in order to eliminate erroneous LiDAR returns above occurring tree heights. Note that average vegetation height is not equivalent to canopy height (height of returns at the top of the canopy), but is instead affected by all returns within a 25 m pixel throughout the vertical vegetation column between 0.4 m and 55 m. Vegetation cover was calculated as all first returns above 40 cm divided by all first returns, which indicates how much of a 25 m cell is covered by vegetation taller than 40 cm. Foliage height diversity (FHD) describes how LiDAR returns are distributed among 5 m vertical bins, and was calculated as the Shannon Index $H = -\sum p_i \ln (p_i)$, where p_i is the proportion of returns in bin i relative to all returns. Vertical coefficient of variation was calculated as the coefficient of variation of all returns (the standard deviation divided by the mean height of all returns).

2.2.3 Light availability along LiDAR-derived predictors

We here outline how we expected light-availability in a forest stand to change along the LiDAR-derived predictors (see also Figure 1). We expected light availability to decrease with increasing average vegetation height because maximal light availability for the understorey is

reached when there are no or just a few large trees, whereas in forest stands with high, closed canopies, light availability for the understorey is low (Figure 1a). Light availability within forest stand is expected to decrease with increasing vegetation cover (Figure 1b). A low vertical coefficient of variation is caused by low variation of returns in high canopies, a situation that leads to low light availability in a stand. Conversely, one finds high vertical coefficients of variation if vertical variation is high relative to a low average canopy height. Consequently, we expected light availability on low vegetation heights to increase along the vertical coefficient of variation (Figure 1c). FHD captures how returns are distributed among vertical bins of vegetation height. It is lowest if all returns are concentrated in one or a few bins, which is the case in very low vegetation, where a lot of light is available. Highest FHD is expected if returns are evenly distributed across all height-bins, offering less light within the stand than the low vegetation that leads to high FHD. Therefore, we expect light availability to decrease along FHD (Figure 1d).

2.3 Distribution modeling

2.3.1 Variable selection

Our hypotheses required to fit two types of models for each species: one with only climatic, topographical, and soil predictors, and one including LiDAR-derived predictors. We selected the six most important but only weakly correlated variables for each type of model using a deterministic approach. We first ran a logistic regression for each species and predictor with a linear and quadratic term, and ranked each predictor's predictive power using the average out-of-bag true skill statistic (TSS; Allouche et al., 2006) from a 20-fold cross validation. Starting from the best performing predictor (rank one), we iteratively removed highly correlated predictors with a Pearson correlation coefficient $|r| > 0.7$ in order to avoid multi-collinearity (Dormann et al., 2013) before selecting the next best predictor. For the models without LiDAR data, the six best-ranked, uncorrelated, predictors describing climate,

topography, and soil were chosen, separately for each species. For the models that included LiDAR data, the three best LiDAR-derived predictors were given the best ranks and complemented with the three best-ranked predictors out of the climatic, topographic, and soil predictor group. This procedure ensured that both models types (with and without LiDAR) had the same number of predictors (6) and this means that the three LiDAR predictors were included at the cost of three abiotic predictors. Table A4 lists the combination of variables used for each type of model and species.

2.3.2 Modeling procedure

In line with current standards (Araújo et al., 2019), we used an ensemble of models to assess predictive performance of SDMs with and without LiDAR data. For each species and predictor-set we used the following five algorithms and packages in the R statistical software (Version 3.4.4, R Core Team, 2018): generalized linear model (GLM, Nelder and Wedderburn, 1972) and generalized additive model (GAM, Hastie and Tibshirani, 1990; using *mgcv*, Wood, 2006) with binomial error distribution and logit link, random forest (RF, Breiman, 2001; using *randomForest*, Liaw and Wiener, 2002), artificial neural network (ANN, Ripley, 1996; using *nnet*, Venables and Ripley, 2002) and MaxEnt (using *dismo*, Hijmans et al., 2017; Phillips et al., 2006). GLMs were fitted using linear and quadratic terms. GAMs were fitted with up to four degrees of freedom (k=5). Both RFs and ANN were tuned to optimize parameter settings. For RFs, we optimized number of trees selecting from 500, 1000, or 2000 trees, chose the best-performing minimal size of terminal nodes from two, three, or five, and chose the optimal number of candidate variables at each split from one, two or four variables. For ANNs, we chose the best combination of number of hidden layers (two, four, six, eight, or ten) and weight decays (0.001, 0.01, 0.05, 0.1, 0.25). MaxEnt models were fitted with default settings, except that a minimum of 100 observations was required to include hinge features, and a minimum of 150 observations to include product features.

2.3.3 Model performance

We assessed model performance via cross-validation using a repeated split-sample approach. For each repeat, we randomly split the NFI data into 70 % training, and 30 % testing data. Each of the five models was fitted on the training data, and the testing data was used to predict the probability of occurrence for the given species. These probabilities were transformed into binary predictions of presence/absence by optimizing a threshold that maximized TSS. We then calculated TSS on the held-out test data (TSS_{CV}) for each of the five models, eight species, two sets of variables, and 20 cross-validation repeats as the basis to test hypotheses H1 to H3.

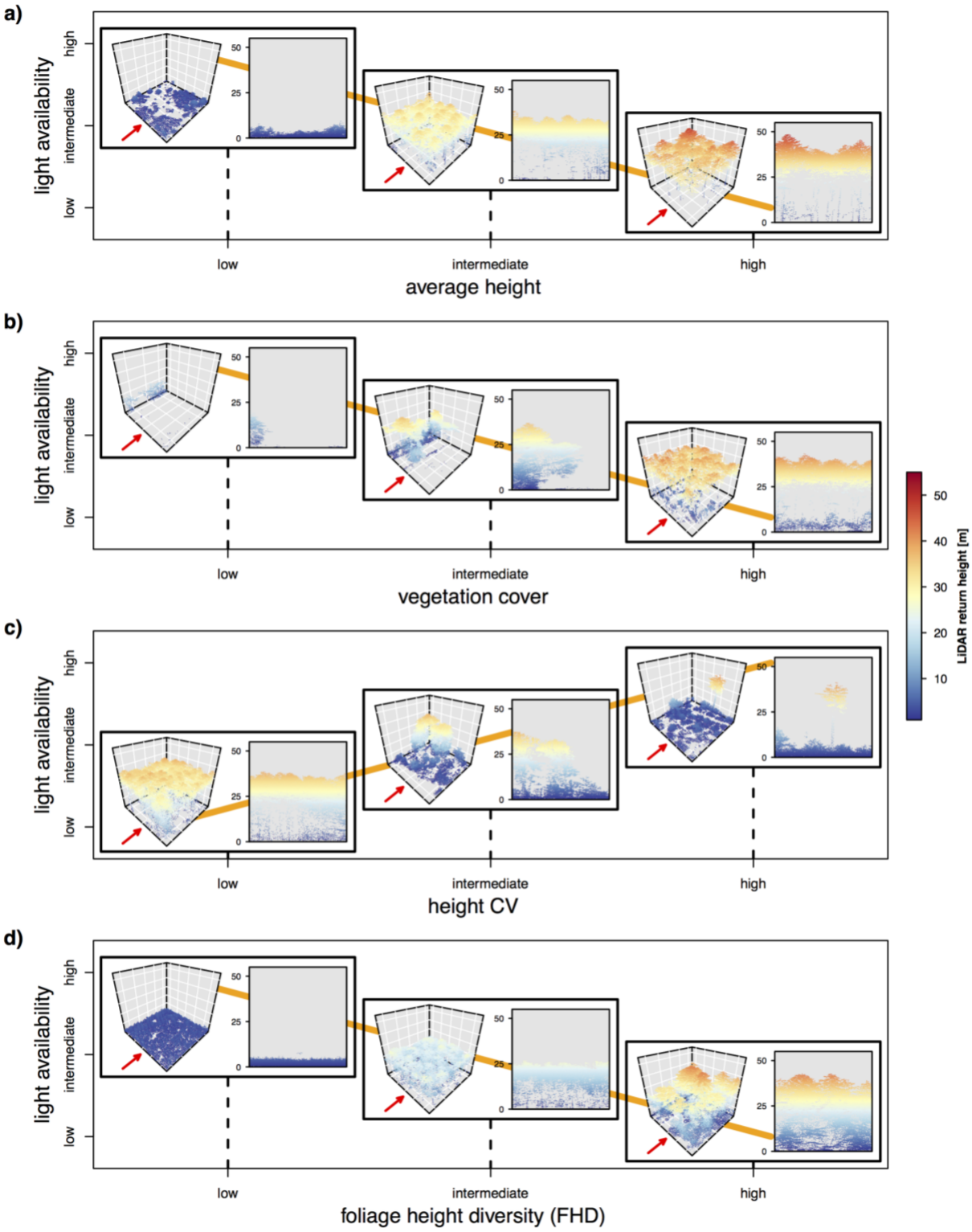

250

251 **Figure 1** Illustration of expected light availability(orange lines in the background) within a forest stand along
252 the four LiDAR-derived predictors used in this study. Note that the expected light availability here only
253 illustrates the general expected trend (actual light availability could to display a more complex response). The
254 inset boxes illustrate exemplary LiDAR point clouds of a 25 m pixel along three points of the LiDAR-derived
255 predictor (indicated by black dashed lines). Each inset box shows a subplot in 3D on the left, and a second

subplot in 2D with the view from the perspective illustrated by the red arrows. The colors of LiDAR points illustrate their return height above ground (see color legend).

2.4 Hypothesis Testing

2.4.1 Statistical analyses

We used a mixed effect model in order to test hypotheses H1, H2 and H3. Predictive performance of models (the TSS_{CV} values) constituted the response in this mixed effect model. Predictor-set (SDMs without vs. SDMs including LiDAR-derived predictors), life form (shrubs vs. trees) and light requirement (shade-tolerant vs. light-demanding) were included as fixed effects. We further included the interactions between predictor-set and life form, as well as between predictor-set and light requirement. Hypothesis H1 predicts a positive intercept for the predictor-set "with LiDAR". The interactions between predictor-set and life form, and between predictor-set and light requirement were included to test hypothesis H2 and H3. Both these hypotheses predict that the increase in predictive performance (not its absolute value) changes with a functional attribute of the species. Hence, in the statistical model we have to inspect the interactions that modulate the increase in predictive performance, and not the intercepts (the absolute values) themselves. H2 predicts a negative coefficient for the interaction between predictor-set and life form (trees vs. shrubs), and hypothesis H3 predicts a negative coefficient for the interaction between predictor-set and light requirement (shade-tolerant vs. light-demanding). We included a random intercept for each species, model algorithm and cross-validation repeat to account for repeated measurements and for differences in model performance between species and models. We tested for significance of the effects by inspecting the 95 % confidence intervals (CIs) of a posterior sample of the effects. These samples were generated by sampling the estimated distribution of the effect (given by the point estimate and its standard error). The mixed

model was built using the *lme4* R-package (Bates et al., 2015), the CIs were computed using the *arm* R-package (Gelman and Su, 2018).

2.4.2 Response curves

We generated partial response curves of how the probability of occurrence changes along the LiDAR-derived predictors to test hypothesis H4. Generally, partial response curves are produced by calculating the predicted probability of occurrence along the focal predictor, while all other predictors are fixed (here: at their mean). In our study, we generated ensemble response curves, where the partial responses of the five models along each LiDAR-derived predictor was averaged. Models that performed better thereby received more weight than models with lesser performance (average TSS_{CV} values were used as weights). We used the weighted standard deviation of the predicted probabilities across the five models to illustrate uncertainty among the five model algorithms. The generated response curves were used to assess whether the responses of light-demanding vs. shade-tolerant species show the opposing patterns, as predicted by hypothesis H4.

3 Results

On average, predictive performance of models (TSS_{CV}) was 0.45 (±0.13; standard deviation) across all species, models, and cross-validation repeats when LiDAR data were not included. Performance across models was similar, with RFs (0.46±0.12), GAMs (0.46±0.12) and Maxent models (0.46±0.12) performing better than GLMs (0.45±0.14) and ANNs (0.44±0.14). *Fagus sylvatica* reached the best TSS_{CV} (0.65 ±0.02), whereas *Populus tremula* only reached 0.23 (±0.08). When including LiDAR-derived predictors, the changes in TSS_{CV} ranged from −0.18 to 0.27 in absolute terms, whereas relative changes ranged from −48.51 % to 501.94 % (negative values indicate that models without LiDAR data performed better).

303 The functional groups reacted differently to the inclusion of LiDAR data (Figure 2). The
304 strongest increase in TSS median was 7.5 % (quartile range: 0.7 to 15.8 %) for light-
305 demanding shrubs (*J. communis* and *P. spinosa*), and similar for light-demanding trees 6.9 %
306 (from 0.4 for *P. tremula* to 23.2 for *P. sylvatica*). In contrast, we observed a decrease in
307 median TSS in shade-tolerant shrubs (−4.2; −10.7 to 6.2 %, *D. mezerum* and *L. nigra*) and
308 trees (−6.3 %; −10 to −1.1 %, *F. sylvatica* and *P. abies*). Accordingly, models for light-
309 demanding species increased in performance by 7.18 % (0.60 to 18.26 %), whereas those for
310 shade-tolerant species decreased in performance by −5.36 % (−10.20 to 1.35 %). When
311 inspecting life form, we observed that including LiDAR-derived predictors did only
312 marginally affect models for trees (0.05 %; −7.36 to 7.81 %), but had a higher effect on
313 shrubs (2.32 %; −6.16 to 13.56 %).
314 Models that included LiDAR-derived predictors performed better in five out of eight species
315 compared to the models without LiDAR data. *F. sylvatica* and *L. nigra* showed a decrease in
316 predictive performance when including LiDAR data, and for *P. abies* predictive performance
317 did not differ. Nevertheless, species varied considerably in how model performance changed
318 with inclusion of LiDAR data. The two extreme examples included trees: *P. tremula* had a
319 median increase of 23.3 % (4.6 to 51.6 %) in TSS_{CV}, whereas model performance for *F.*
320 *sylvatica* decreased by −9.1 % (−11.1 to −7.4 %). The difference between extremes was
321 smaller for shrubs: TSS_{CV} for *L. nigra* decreased by −8.0 % (−12.4 to −4.4 %) and increased
322 for *J. communis* by 13.8 % (2.9 to 23.4 %). For more details on species-specific results see
323 Figure 2 and Table A5.
324 Analyses indicated that both the main effect for predictor-set as well as its interactions with
325 life form and light requirement were significant (Table 2). In contrast, the main effects for
326 life form and light requirement were not significant. The main effect of predictor-set
327 indicated that TSS_{CV} increased for light-demanding shrubs when including LiDAR-derived

predictors. This increase was, however, reduced for tree species, especially so for shade-tolerant species, as indicated by the two negative interaction terms. The large effect for the interaction between predictor-set and light requirement means that model performance estimates of models with LiDAR data for shade tolerant species are lower than for light-demanding species (see the model coefficients in the central panels of Figure 2).

Table 2 The results for the fixed effects of the mixed model that statistically tested whether the predictive performance of SDMs (measured as TSS_{CV}) changed as predicted by hypotheses H1, H2 and H3. The first column gives the estimate the second and third column define the lower and upper limits of the 95 % Confidence Intervals (CI). Significant effects (i.e. CIs do not include zero) in bold. Note that we highlight in the first column in brackets what levels the fixed effects take (the levels mentioned for the intercept constitute the base levels).

	estimate	lower CI	upper CI
Intercept			
(no LiDAR, shrubs, light-demanding)	**0.426**	0.272	0.589
predictor-set			
(with LiDAR)	**0.047**	0.039	0.054
life form			
(trees)	−0.001	−0.192	0.189
light requirement			
(shade-tolerant)	0.051	−0.128	0.239
predictor-set : life form			
(with LiDAR, trees)	**−0.016**	−0.024	−0.006
predictor-set : light requirement			
(with LiDAR, shade-tolerant)	**−0.061**	−0.069	−0.052

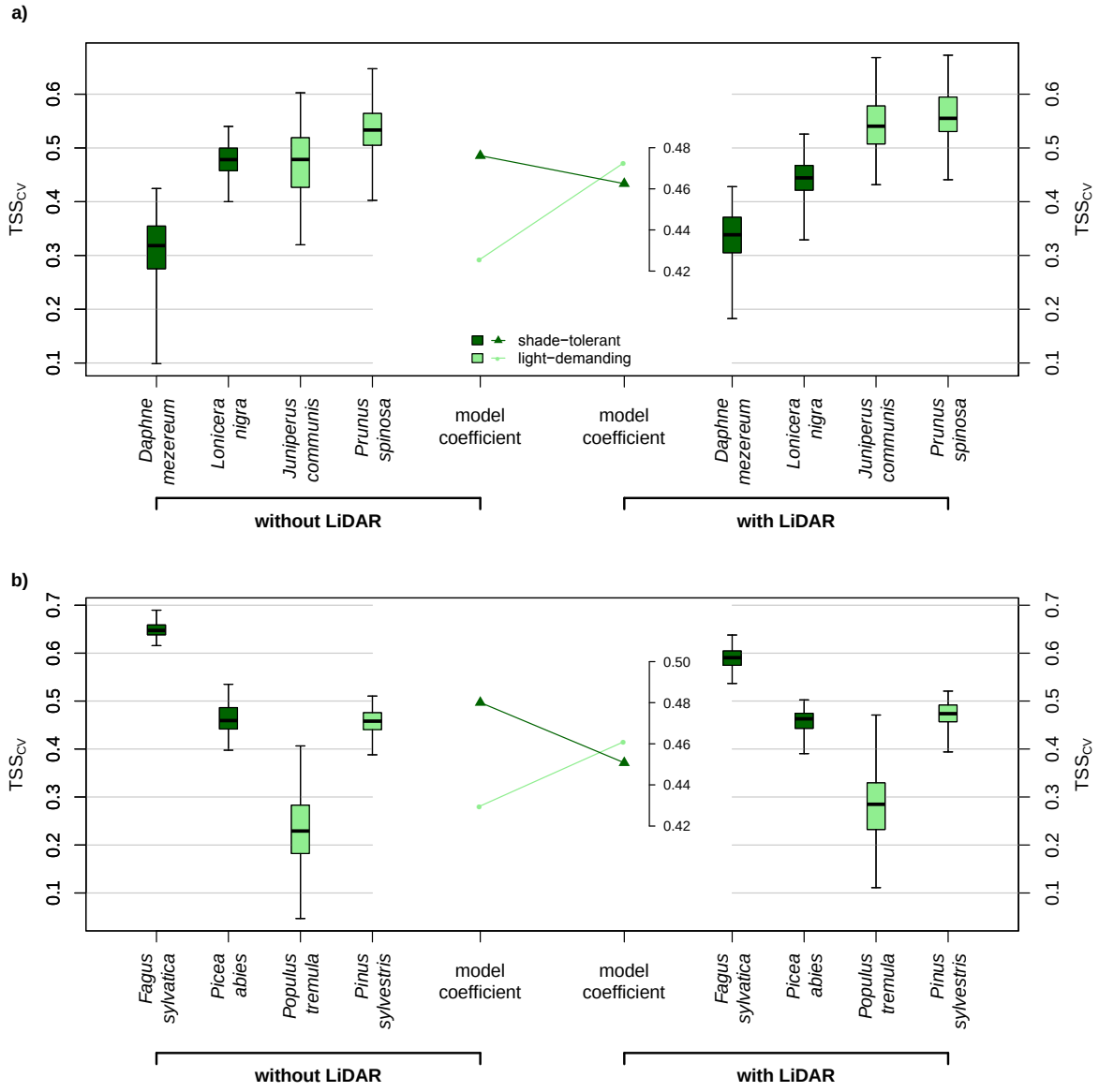

Figure 2 Summary figure of results for shrubs in a) and trees in b). The left panels show model performance (TSS_{CV}) for models without the use of LiDAR data, right panels show model performance for models that included LiDAR-derived predictors. The central panels (with inset axes for TSS_{CV}) illustrate the interaction effects as estimated by the mixed effect model, highlighting that the inclusion of LiDAR-derived predictors increases model performance for light-demanding species (light green), but decreases model performance for shade-tolerant species (dark green).

The majority of ensemble response curves for light-demanding species indicated that the probability of occurrence for a given species decreased along any of the four LiDAR-derived predictors (see examples in Figure 3 and the complete set of response curves in Figure A1 and Figure A2), except along foliage height diversity which displays a hump-shaped pattern for *J. communis* and *P. sylvestris* and an invariant response for *P. spinosa*. *P. sylvestris* further exhibits a positive response along vegetation cover and hump-shaped responses along average canopy height, which is diverging from the most common pattern of light-demanding species (Figure 3). Most ensemble response curves for shade-tolerant species showed an opposite pattern: the probability of occurrence of most species increased along the LiDAR-derived predictors (see the examples in Figure 3). The exceptions here concern average vegetation height and canopy variation for *D. mezereum* (decreasing probability of occurrence and invariant response, respectively), as well as vegetation cover for *F. sylvatica*, FHD for *L. nigra*, and average vegetation height for *P. abies* (all hump-shaped, see examples in Figure 3).

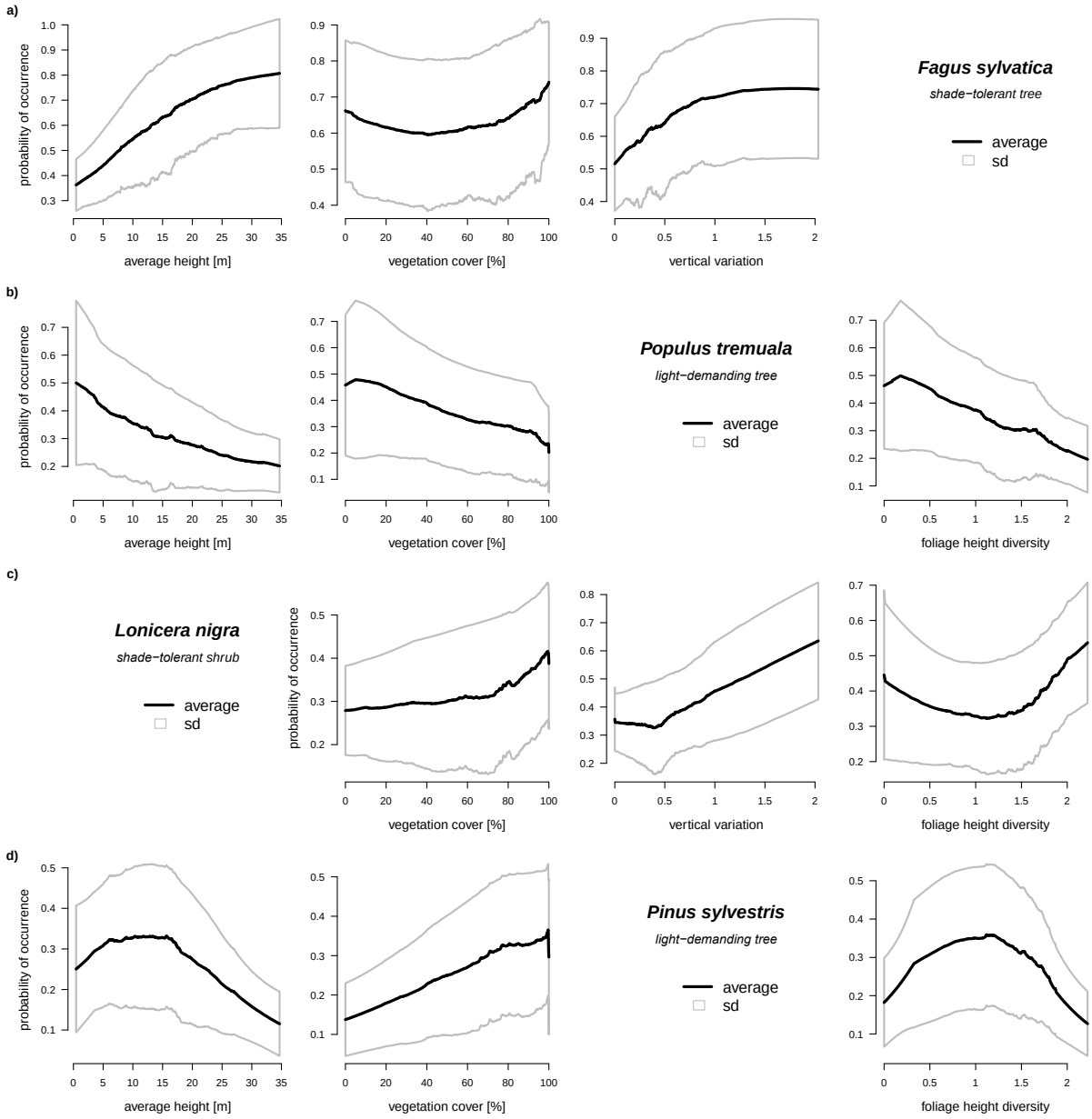

365

366 **Figure 3** Expected (a, b) and unexpected (c, d) partial response curves for the shade-tolerant *F. sylvatica* (a)
367 and *L. nigra* (c) and light-demanding *P. tremula* in (b) and *P. sylvestris* in (d). Solid black lines indicate the
368 weighted ensemble responses and grey polygons reflect the weighted standard deviation across the five model
369 algorithms. Note that we assumed light availability to decrease with increasing average vegetation height,
370 vegetation cover and FHD, and to increase with vertical coefficient of variation. Also note that the response of
371 *F. sylvatica* along vegetation cover is not as expected, whereas the response of *L. nigra* along vegetation cover
372 is as expected. Partial response curves for each species and model algorithm along all LiDAR-derived predictors
373 are displayed in Figure A1 and Figure A2.

374

4 Discussion

Our study showed that the inclusion of LiDAR-derived predictors in SDMs is beneficial for light-demanding species, especially shrubs. Results also indicated that light-demanding and shade-tolerant species generally exhibit opposing responses along LiDAR-derived predictors. SDMs and resulting distribution maps for woody species can thus be improved by using LiDAR data, especially when following a set of recommendations based on the life form and light requirements of species.

4.1 LiDAR and model performance

Our results from the statistical analyses indicate that LiDAR data does increase model performance, and that this increase is less pronounced in shade tolerant species and in tree species, congruent with the predictions from hypotheses H1 to H3. A closer inspection of the results, however, reveals variation across the investigated species. In line with our hypothesis H3, model performance of all four light-demanding species increased when including LiDAR-derived predictors, but only one shade-tolerant species exhibited the same response. We argue that our structural predictors derived from LiDAR data captured substantial aspects of the limiting light availability in forests and thus are valuable predictors in SDMs of light-demanding species. This is also in accordance with the literature of SDMs that included forest structure derived from LiDAR data for animal species which depend on open forest stands (see Davies and Asner, 2014 for examples).

Shade-tolerant species, on the other hand, are less limited by light conditions, and their distribution could be more affected by other environmental factors such as climate or soil properties. In our study, the inclusion of LiDAR-derived predictors was at the cost of excluding such environmental factors. Apparently, this cost was higher than the benefit from including forest structural data, leading the models with LiDAR data to perform worse than the models based solely on climate, topography and soil characteristics for most shade-

tolerant species. The only exception is *D. mezereum*, where model performance increases by 10% on average. The response curve for *D. mezereum* along the vegetation cover gradient is similar to those of other shade-tolerant species, its response along average height and canopy variation, however, rather parallels those from light-demanding species (Figure A1). Further investigations that go beyond the scope of this study would be required to assess if the observed similarity to response curves of light-demanding species is responsible for the exceptionally high increase in model performance of *D. mezereum* when including LiDAR-derived predictors.

We also found differences between life forms in how model performance increased with LiDAR-derived predictors. In line with the prediction of our hypothesis H2, we found that models for tree species profit less from LiDAR-derived predictors than models for shrub species. Indeed, we find a higher increase in model performance for light-demanding shrub species than for light-demanding tree species (light green model coefficients in Figure 2). Shrubs are part of the understorey, and as such are more affected by the overstorey forest structure than the investigated tree species that grow tall enough to become part of the upper canopy, where light is not a limiting factor. The significant interaction also indicates a stronger decrease in model performance for shade-tolerant tree species than for shrubs (dark green model coefficients in Figure 2). This is likely the consequence of the large drop in model performance for *F. sylvatica* when LiDAR-derived predictors are part of the predictor-set (a median decrease of −9.1 %, Table A5). Across a large part of the Swiss lowlands, *F. sylvatica* is the most abundant and dominant tree species (Brzeziecki et al., 1993; Ellenberg, 1988; Keller et al., 1998). Meier and colleagues (2011) found that beech dominance against its main competitors across Europe is influenced by climate, specifically temperature (degree day sum) and summer precipitation. It is striking that the LiDAR-derived predictors replaced, beside a topographic predictor, precipitation of the driest month and summer/winter ratio of

precipitation (Table A4). Hence, the large decrease in model performance is most likely caused by the substitution of such informative climatic predictors with LiDAR-derived predictors due to the design of our study, which required the number of predictors to be constant across the predictor-sets. However, when constructing the best possible SDM for *F. sylvatica* with the data at hand (an inventory with thousands of high-quality presence/absence observations), we would rather add LiDAR-derived predictors to a chosen set of climatic, topographic, and soil predictors instead of replacing any of these abiotic predictors.

4.2 Responses along LiDAR predictors

We found that the majority of the partial responses along LiDAR-derived predictors follow the patterns that we predicted based on how we expect light-availability in a forest stand to change along the LiDAR-derived predictors. Consistent with this, we found opposing responses along most LiDAR-derived predictors for shade-tolerant vs. light-demanding species, just as predicted by hypothesis H4. These opposing responses support our assumption that the chosen predictors indeed capture relevant aspects of light availability in forest stands. However, it is important to note that the LiDAR-derived predictors we used to describe forest structure can also be proxies for other factors affecting the occurrence of woody species. For example, shrubs in the understorey are not only affected by light availability, but also by the distinct understorey microclimate (Bramer et al., 2018) that was potentially captured by our structural predictors derived from LiDAR data (Frey et al., 2016; Zellweger et al., 2018).

The fact that our LiDAR-derived predictors are potentially correlated with additional, unobserved environmental variables could potentially explain some of the unexpected partial responses. The “chicken and egg” issue raised by Bradley et al. (2012) in combination with the fact that light requirements of tree species change with their life stage offers an alternative explanation. For example, we observed a positive association of *P. sylvestris* occurrence

probability with vegetation cover, even though one would expect a light-demanding species to show the opposite trend. However, the light requirement is highest at the rejuvenation stage, whereas an adult *P. sylvestris* tree reaches the canopy, where light is not a limiting resource. And at this adult stage, the full-grown tree contributes a lot to the vegetation cover of its forest stand, which in turn determines how suitable that forest stand will be as determined to the SDM (high, according to partial response of *P. sylvestris* along vegetation cover). Finding detailed explanations for the shapes of all partial responses along the LiDAR-derived predictors is clearly beyond the scope of our study. And the fact that we don't have adequate explanations, for example, for the unexpected response patterns of *P. sylvestris* or the u-shaped response of *F. sylvatica* along vegetation cover suggests that further research with targeted analyses is needed to address these issues.

4.3 Challenges and Opportunities

In general, it is important to recall the partial circularity inherent to models that use LiDAR-derived predictors to model a state of woody species distribution within a stand dynamic process: LiDAR data picks up vegetation structural attributes that are on the one hand important in determining their distribution, but on the other hand are also affected by their inherent distribution. In accordance with earlier recommendations (Bradley et al., 2012), we caution against interpreting the derived maps as the potential distribution of a species. Further research is needed to better disentangle the chicken from the egg, i.e., to disentangle the effects of trees on canopy structure form the effects of canopy structure on the distribution of tree species. Separating tree species observations into under- and overstorey canopy individuals, potentially also in life stages (seedlings, young trees, canopy trees) could shed light on how and when during their life cycle tree species are affected by the canopy structure, and how and when they are affecting the canopy structure.

Focusing on the specifics of our study, we see a possible limitation in the number of species that we analyzed. We are confident that our results represent general trends for plant functional groups, but our results also indicate that single species can exhibit unexpected responses (e.g., *P. sylvestris*, *D. mezereum*). Therefore, instead of deciding whether or not to include LiDAR data in SDMs of woody species simply according to their plant functional group, we suggest to test if predictive performance of SDMs indeed increases when including LiDAR-derived predictors. In addition, we would like to point out that the absolute changes in model performance in our comparisons, as assessed by TSS_{CV} are rather small. Average absolute changes per species range from 0.006 to 0.07, with a mean of 0.04. However, especially the light-demanding shrubs show increases of up to >0.15 for certain cross-validation repeats, which we certainly consider worthwhile. Further research is needed to study if the small absolute differences could be explained by the design of our study and turn out to increase when the addition of LiDAR-derived predictors does not replace abiotic predictors.

We anticipate that positive effects of LiDAR-derived predictors on SDMs could also be found for non-woody species such as herbaceous species or bryophytes and lichens that inhabit forests. Modelling of such species by means of LiDAR data would not be affected by the chicken-egg problem because those species groups hardly affect the forest structure as characterized by LiDAR-derived predictors. However, non-woody species inhabiting the understorey strongly depend on light conditions. Indeed, recent studies show that LiDAR-derived data are well suited to approximate light-demands of herbaceous understory communities (Alexander et al., 2013).

Remote sensing products already have proven their value in the management of invasive species (e.g., Hantson et al., 2012; Müllerová et al., 2017), and we expect that LiDAR-derived predictors that inform on light availability also have the potential to improve maps of

the potential distributions of invasives. Such maps could, for example, identify potential hotspots for the establishment of black-listed species that are especially competitive under favorable light conditions and (start to) inhabit Swiss forests, such as Black locust (*Robinia pseudoacacia*) in light forests or Cherry laurel (*Prunus laurocerasus*) along forest edges (Delarze et al., 2015; Info Flora, 2014).

4.4 Recommendations for Application

Our study set out to discover if LiDAR data is useful when modeling the distribution of woody species, and to confirm predicted differences between functional groups of woody species based on specific hypotheses. Our recommendations are based on our results that show that LiDAR-derived predictors generally increase model performance and are especially useful when modeling the distribution of light-demanding shrubs.

We emphasize that the inclusion of LiDAR-derived predictors prevents the possibility to project the models to future conditions, simply because structural data of future forest stands cannot be acquired. However, using forest structural data in distribution models fitted in one area may allow to project models to new areas, given LiDAR data is available for these new areas in a similar quality. Note that we suggest to apply block cross-validation in order to assess the transferability of the fitted SDMs (Roberts et al., 2017) when aiming for projection to another area.

When aiming for producing the best possible maps for management purposes, we recommend to include LiDAR-derived predictors into SDMs for woody species if the species is light-demanding, especially so if shrubs are concerned. For such species, LiDAR data exhibit considerable potential to improve species distributions maps. If occurrence data is limiting the number of predictors that can be included in SDMs, we warn against a non-reflected inclusion of LiDAR-derived predictors. The case of *F. sylvatica* exemplifies that replacing important abiotic predictors with LiDAR-derived predictors can harm the performance of

SDMs. Hence, we recommend to test the predictive performance of models with/without LiDAR-derived predictors when the number of predictors is limited or to apply ensembles of small models (Breiner et al., 2015). Our recommendations provide a basis how remote-sensing technologies and highly resolved parameters of vegetation structure can increase the accuracy of spatially explicit models for woody species. As such, these models and resulting maps have the potential to inform multifunctional, biodiversity-friendly stand management.

Acknowledgements

We are grateful to Meinrad Abegg for providing the Swiss NFI data and Michael Nobis for his support on the data from Flora Indicativa. ROW and AB acknowledge funding from the Swiss National Forest Inventory run by the Swiss Federal Office for the Environment FOEN and the Swiss Federal Research Institute WSL.

References

Alexander, C., Moeslund, J.E., Bøcher, P.K., Arge, L., Svenning, J.C., 2013. Airborne laser scanner (LiDAR) proxies for understory light conditions. Remote Sens. Environ. 134, 152–161. https://doi.org/10.1016/j.rse.2013.02.028

Allouche, O., Tsoar, A., Kadmon, R., 2006. Assessing the accuracy of species distribution models: prevalence, kappa and the true skill statistic (TSS). J. Appl. Ecol. 43, 1223–1232. https://doi.org/10.1111/j.1365-2664.2006.01214.x

Alonzo, M., Bookhagen, B., Roberts, D.A., 2014. Remote Sensing of Environment Urban tree species mapping using hyperspectral and lidar data fusion. Remote Sens. Environ. 148, 70–83. https://doi.org/10.1016/j.rse.2014.03.018

Araújo, M.B., Anderson, R.P., Márcia Barbosa, A., Beale, C.M., Dormann, C.F., Early, R.,

546 Garcia, R.A., Guisan, A., Maiorano, L., Naimi, B., O'Hara, R.B., Zimmermann, N.E.,
547 Rahbek, C., 2019. Standards for distribution models in biodiversity assessments. Sci.
548 Adv. 5, eaat4858. https://doi.org/10.1126/sciadv.aat4858

549 Ares, A., Neill, A.R., Puettmann, K.J., 2010. Understory abundance, species diversity and
550 functional attribute response to thinning in coniferous stands. For. Ecol. Manage. 260,
551 1104–1113. https://doi.org/10.1016/j.foreco.2010.06.023

552 Artuso, R., Bovet, S., Streilein, A., 2003. Practical methods for the verification of
553 countrywide terrain and surface models, in: IInternational Archives of Photogrammetry
554 and Remote Sensing, Vol XXXIV, Part 3/W13. pp. 0–5.

555 Baltensweiler, A., Walthert, L., Ginzler, C., Sutter, F., Purves, R.S., Hanewinkel, M., 2017.
556 Terrestrial laser scanning improves digital elevation models and topsoil pH modelling in
557 regions with complex topography and dense vegetation. Environ. Model. Softw. 95,
558 13–21. https://doi.org/10.1016/j.envsoft.2017.05.009

559 Barbier, S., Gosselin, F., Balandier, P., 2008. Influence of tree species on understory
560 vegetation diversity and mechanisms involved-A critical review for temperate and
561 boreal forests. For. Ecol. Manage. 254, 1–15.
562 https://doi.org/10.1016/j.foreco.2007.09.038

563 Bartels, S.F., Chen, H.Y.H., 2010. Is understory plant species diversity driven by resource
564 quantity or resource heterogeneity? Ecology 91, 1931–1938.
565 https://doi.org/10.1890/09-1376.1

566 Bates, D., Mächler, M., Bolker, B., Walker, S., 2015. Fitting Linear Mixed-Effects Models
567 Using lme4. J. Stat. Softw. 67. https://doi.org/10.18637/jss.v067.i01

568 Bouvier, M., Durrieu, S., Gosselin, F., Herpigny, B., 2017. Use of airborne lidar data to
569 improve plant species richness and diversity monitoring in lowland and mountain
570 forests. PLoS One 12, e0184524. https://doi.org/10.1371/journal.pone.0184524

571 Bradley, B.A., Olsson, A.D., Wang, O., Dickson, B.G., Pelech, L., Sesnie, S.E., Zachmann, L.J.,
572 2012. Species detection vs. habitat suitability: Are we biasing habitat suitability models
573 with remotely sensed data? Ecol. Modell. 244, 57–64.
574 https://doi.org/10.1016/j.ecolmodel.2012.06.019

575 Bramer, I., Anderson, B.J., Bennie, J., Bladon, A.J., Frenne, P. De, Hemming, D., Hill, R.A.,
576 Kearney, M.R., Christian, K., Korstjens, A.H., Lenoir, J., Maclean, I.M.D., Marsh, C.D.,
577 Morecroft, M.D., Ohlem, R., Slater, H.D., Suggitt, A.J., Zellweger, F., Gillingham, P.K.,
578 2018. Advances in Monitoring and Modelling Climate at Ecologically Relevant Scales 58.
579 https://doi.org/10.1016/bs.aecr.2017.12.005

580 Brandtberg, T., 2007. Classifying individual tree species under leaf-off and leaf-on conditions
581 using airborne lidar. ISPRS J. Photogramm. Remote Sens. 61, 325–340.
582 https://doi.org/10.1016/j.isprsjprs.2006.10.006

583 Brassel, P., Lischke, H. (Eds.), 2001. Swiss National Forest Inventory:Methods and Models of
584 the Second Assessment. SwissFederal Research Institute WSL, Birmendorf.

585 Breiman, L., 2001. Random Forests. Mach. Learn. 45, 5–32.
586 https://doi.org/10.1023/a:1010933404324

587 Breiner, F.T., Guisan, A., Bergamini, A., Nobis, M.P., 2015. Overcoming limitations of
588 modelling rare species by using ensembles of small models. Methods Ecol. Evol. 6,
589 1210–1218. https://doi.org/10.1111/2041-210X.12403

590 Brzeziecki, B., Kienast, F., Wildi, O., 1993. A simulated map of the potential natural forest
591 vegetation of Switzerland. J. Veg. Sci. 4, 499–508. https://doi.org/10.2307/3236077

592 Camathias, L., Bergamini, A., Küchler, M., Stofer, S., Baltensweiler, A., 2013. High-resolution
593 remote sensing data improves models of species richness. Appl. Veg. Sci. 16, 539–551.
594 https://doi.org/10.1111/avsc.12028

595 Ciuti, S., Tripke, H., Antkowiak, P., Gonzalez, R.S., Dormann, C.F., Heurich, M., 2018. An
596 efficient method to exploit LiDAR data in animal ecology. Methods Ecol. Evol. 9, 893–
597 904. https://doi.org/10.1111/2041-210X.12921

598 Clawges, R., Vierling, K., Vierling, L., Rowell, E., 2008. The use of airborne lidar to assess
599 avian species diversity, density, and occurrence in a pine/aspen forest. Remote Sens.
600 Environ. 112, 2064–2073. https://doi.org/10.1016/j.rse.2007.08.023

601 Conrad, O., Bechtel, B., Bock, M., Dietrich, H., Fischer, E., Gerlitz, L., Wehberg, J., Wichmann,
602 V., Böhner, J., 2015. System for Automated Geoscientific Analyses (SAGA) v. 2.1.4.
603 Geosci. Model Dev. 8, 1991–2007. https://doi.org/10.5194/gmd-8-1991-2015

604 Davies, A.B., Ancrenaz, M., Oram, F., Asner, G.P., 2017. Canopy structure drives orangutan
605 habitat selection in disturbed Bornean forests. Proc. Natl. Acad. Sci. 201706780.
606 https://doi.org/10.1073/pnas.1706780114

607 Davies, A.B., Asner, G.P., 2014. Advances in animal ecology from 3D-LiDAR ecosystem
608 mapping. Trends Ecol. Evol. 29, 681–691. https://doi.org/10.1016/j.tree.2014.10.005

609 Delarze, R., Gonseth, Y., Eggenberger, S., Vust, M., 2015. Lebensräume der Schweiz. ott
610 verlag, Bern.

611 Dormann, C.F., Elith, J., Bacher, S., Buchmann, C., Carl, G., Carré, G., Marquéz, J.R.G., Gruber,

612 B., Lafourcade, B., Leitão, P.J., Münkemüller, T., McClean, C., Osborne, P.E., Reineking,
613 B., Schröder, B., Skidmore, A.K., Zurell, D., Lautenbach, S., 2013. Collinearity: a review
614 of methods to deal with it and a simulation study evaluating their performance.
615 Ecography (Cop.). 36, 027–046. https://doi.org/10.1111/j.1600-0587.2012.07348.x

616 Ellenberg, H., 1988. Vegetation Ecology of Central Europe. Cambridge University Press,
617 Cambridge.

618 Farrell, S.L., Collier, B.A., Skow, K.L., Long, A.M., Campomizzi, A.J., Morrison, M.L., Hays, K.B.,
619 Wilkins, R.N., 2013. Using LiDAR-derived vegetation metrics for high-resolution, species
620 distribution models for conservation planning. Ecosphere 4, 1–18.
621 https://doi.org/10.1890/ES12-000352.1

622 Frey, S.J.K., Hadley, A.S., Johnson, S.L., Schulze, M., Jones, J.A., Betts, M.G., 2016. Spatial
623 models reveal the microclimatic buffering capacity of old-growth forests. Sci. Adv. 2,
624 e1501392. https://doi.org/10.1126/sciadv.1501392

625 Froidevaux, J.S.P., Zellweger, F., Bollmann, K., Jones, G., Obrist, M.K., 2016. From field
626 surveys to LiDAR: Shining a light on how bats respond to forest structure. Remote Sens.
627 Environ. 175, 242–250. https://doi.org/10.1016/j.rse.2015.12.038

628 Gelman, A., Su, Y.-S., 2018. arm: Data Analysis Using Regression and Multilevel/Hierarchical
629 Models.

630 Guisan, A., Thuiller, W., 2005. Predicting species distribution: offering more than simple
631 habitat models. Ecol. Lett. 8, 993–1009. https://doi.org/10.1111/j.1461-
632 0248.2005.00792.x

633 Guisan, A., Zimmermann, N.E., 2000. Predictive habitat distribution models in ecology. Ecol.

634 Modell. 135, 147–186. https://doi.org/10.1016/S0304-3800(00)00354-9

635 Gustafsson, L., Baker, S.C., Bauhus, J., Beese, W.J., Brodie, A., Kouki, J., Lindenmayer, D.B.,
636 Lõhmus, A., Pastur, G.M., Messier, C., Neyland, M., Palik, B., Sverdrup-Thygeson, A.,
637 Volney, W.J.A., Wayne, A., Franklin, J.F., 2012. Retention Forestry to Maintain
638 Multifunctional Forests: A World Perspective. Bioscience 62, 633–645.
639 https://doi.org/10.1525/bio.2012.62.7.6

640 Halpern, C.B., Halaj, J., Evans, S.A., Dovčiak, M., 2012. Level and pattern of overstory
641 retention interact to shape long-term responses of understories to timber harvest.
642 Ecol. Appl. 22, 2049–2064. https://doi.org/10.1890/12-0299.1

643 Hantson, W., Kooistra, L., Slim, P.A., 2012. Mapping invasive woody species in coastal dunes
644 in the Netherlands: A remote sensing approach using LIDAR and high-resolution aerial
645 photographs. Appl. Veg. Sci. 15, 536–547. https://doi.org/10.1111/j.1654-
646 109X.2012.01194.x

647 Hastie, T.J., Tibshirani, R.J., 1990. Generalized Additive Models. Chapman & Hall/CRC,
648 London.

649 Hijmans, R.J., Phillips, S., Leathwick, J., Elith, J., 2017. dismo: Species distribution modeling.

650 Holmgren, J., Persson, Å., 2004. Identifying species of individual trees using airborne laser
651 scanner. Remote Sens. Environ. 90, 415–423. https://doi.org/10.1016/S0034-
652 4257(03)00140-8

653 Info Flora, 2014. Liste der gebietsfremden invasiven Pflanzen der Schweiz.

654 Isenburg, M., 2015. LAStools – efficient tools for LiDAR processing.

655 Keller, M., 2011. Swiss National Forest Inventory. Manual of the Field Survey 2004–2007.

Swiss Federal Research Institute WSL, Birmensdorf.

Keller, W., Wohlgemuth, T., Kuhn, N., Schütz, M., Wildi, O., 1998. Waldgesellschaften der Schweiz auf floristischer Grundlage. Statistisch überarbeitete Fassung der «Waldgesellschaften und Waldstandorte der Schweiz» von Heinz Ellenberg und Frank Klötzli (1972). Mitt. Eidgenöss. Forsch.anst. Wald Schnee Landsch. 73, 91–357.

Kumar, P., Chen, H.Y.H., Thomas, S.C., Shahi, C., 2010. Linking resource availability and heterogeneity to understorey species diversity through succession in boreal forest of Canada. J. Ecol. 91, 1931–1938. https://doi.org/10.1111/1365-2745.12861

Landolt, E., Bäumler, B., Erhardt, A., Hegg, O., Klötzli, F., Lämmler, W., Nobis, M., Rudmann-Maurer, K., Schweingruber, F.H., Theurillat, J.-P., Urmi, E., Vust, M., Wohlgemuth, T., 2010. Flora Indicativa, 2nd ed. Haupt, Bern.

Lefsky, M.A., Cohen, W.B., Parker, G.G., Harding, D.J., 2002. Lidar Remote Sensing for Ecosystem Studies. Bioscience 52, 19. https://doi.org/10.1641/0006-3568(2002)052[0019:LRSFES]2.0.CO;2

Liaw, A., Wiener, M., 2002. Classification and Regression by randomForest. R News 2, 18–22.

Lindenmayer, D.B., Franklin, J.F., 2002. Conserving Forest Biodiversity: A Comprehensive Multiscaled Approach. Island Press.

Meier, E.S., Edwards, T.C., Kienast, F., Dobbertin, M., Zimmermann, N.E., Edwards Jr, T.C., Kienast, F., Dobbertin, M., Zimmermann, N.E., 2011. Co-occurrence patterns of trees along macro-climatic gradients and their potential influence on the present and future distribution of Fagus sylvatica L. J. Biogeogr. 38, 371–382. https://doi.org/10.1111/j.1365-2699.2010.02405.x

678 Müllerová, J., Bartaloš, T., Brůna, J., Dvořák, P., Vítková, M., 2017. Unmanned aircraft in
679 nature conservation: an example from plant invasions. Int. J. Remote Sens. 38, 2177–
680 2198. https://doi.org/10.1080/01431161.2016.1275059

681 Nelder, J.A., Wedderburn, R.W.M., 1972. Generalized Linear Models. J. R. Stat. Soc. A. 135,
682 370–384. https://doi.org/10.2307/2344614

683 Phillips, S.J., Anderson, R.P., Schapire, R.E., 2006. Maximum entropy modeling of species
684 geographic distributions. Ecol. Modell. 190, 231–259.
685 https://doi.org/10.1016/j.ecolmodel.2005.03.026

686 R Core Team, 2018. R: A language and environment for statistical computing.

687 Ripley, B.D., 1996. Pattern Recognition and Neural Networks. Cambridge University Press,
688 Cambridge.

689 Roberts, D.R., Bahn, V., Ciuti, S., Boyce, M.S., Elith, J., Guillera-Arroita, G., Hauenstein, S.,
690 Lahoz-Monfort, J.J., Schr??der, B., Thuiller, W., Warton, D.I., Wintle, B.A., Hartig, F.,
691 Dormann, C.F., 2017. Cross-validation strategies for data with temporal, spatial,
692 hierarchical, or phylogenetic structure. Ecography (Cop.). 1–17.
693 https://doi.org/10.1111/ecog.02881

694 Shi, Y., Wang, T., Skidmore, A.K., Heurich, M., 2018. Important LiDAR metrics for
695 discriminating forest tree species in Central Europe. ISPRS J. Photogramm. Remote
696 Sens. 137, 163–174. https://doi.org/10.1016/j.isprsjprs.2018.02.002

697 Simonson, W.D., Allen, H.D., Coomes, D.A., 2014. Applications of airborne lidar for the
698 assessment of animal species diversity. Methods Ecol. Evol. 5, 719–729.
699 https://doi.org/10.1111/2041-210X.12219

700 Swisstopo, 2010a. Height Models. Swiss Federal Office of Topography Swisstopo [WWW
701 Document]. URL https://shop.swisstopo.admin.ch/en/products/height_models/dhm25
702 Swisstopo, 2010b. Height Models. Swiss Federal Office of Topography Swisstopo [WWW
703 Document]. URL https://shop.swisstopo.admin.ch/en/products/height_models/alti3D
704 Taki, H., Inoue, T., Tanaka, H., Makihara, H., Sueyoshi, M., Isono, M., Okabe, K., 2010.
705 Responses of community structure, diversity, and abundance of understory plants and
706 insect assemblages to thinning in plantations. For. Ecol. Manage. 259, 607–613.
707 https://doi.org/10.1016/j.foreco.2009.11.019
708 Thers, H., Brunbjerg, A.K., Læssøe, T., Ejrnæs, R., Bøcher, P.K., Svenning, J.-C., 2017. Lidar-
709 derived variables as a proxy for fungal species richness and composition in temperate
710 Northern Europe. Remote Sens. Environ. 200, 102–113.
711 https://doi.org/10.1016/j.rse.2017.08.011
712 Venables, W.N., Ripley, B.D., 2002. Modern Applied Statistics with S, Fourth. ed. Springer,
713 New York.
714 Vierling, L.A., Vierling, K.T., Adam, P., Hudak, A.T., 2013. Using satellite and airborne LiDAR
715 to model woodpecker habitat occupancy at the landscape scale. PLoS One 8.
716 https://doi.org/10.1371/journal.pone.0080988
717 Wilkes, P., Jones, S.D., Suarez, L., Haywood, A., Woodgate, W., Soto-Berelov, M., Mellor, A.,
718 Skidmore, A.K., 2015. Understanding the Effects of ALS Pulse Density for Metric
719 Retrieval across Diverse Forest Types. Photogramm. Eng. Remote Sens. 81, 625–635.
720 https://doi.org/10.14358/PERS.81.8.625
721 Wood, S.N., 2006. Generalized additive models : an introduction with R. Chapman & Hall;

CRC, Boca Raton.

Zellweger, F., Baltensweiler, A., Ginzler, C., Roth, T., Braunisch, V., Bugmann, H., Bollmann, K., 2016. Environmental predictors of species richness in forest landscapes: Abiotic factors versus vegetation structure. J. Biogeogr. 43, 1080–1090. https://doi.org/10.1111/jbi.12696

Zellweger, F., Braunisch, V., Baltensweiler, A., Bollmann, K., 2013. Remotely sensed forest structural complexity predicts multi species occurrence at the landscape scale. For. Ecol. Manage. 307, 303–312. https://doi.org/10.1016/j.foreco.2013.07.023

Zellweger, F., Frenne, P. De, Lenoir, J., Rocchini, D., Coomes, D., 2018. Advances in microclimate ecology arising from remote sensing. Trends Ecol. Evol. xx, 1–15. https://doi.org/10.1016/j.tree.2018.12.012

Zellweger, F., Roth, T., Bugmann, H., Bollmann, K., 2017. Beta diversity of plants, birds and butterflies is closely associated with climate and habitat structure. Glob. Ecol. Biogeogr. 898–906. https://doi.org/10.1111/geb.12598

Zimmermann, N.E., Kienast, F., 1999. Predictive mapping of alpine grasslands in Switzerland : Species versus community approach. J. Veg. Sci. 10, 469–482.

Zurell, D., Zimmermann, N.E., Gross, H., Baltensweiler, A., Sattler, T., Wüest, R.O., 2019. esting species assemblage predictions from stacked and joint species distribution models. J. Biogeogr.

Appendix A: Supplementary Material

Table A1 Full list of candidate species, with the selected species in bold. Note that we generally selected the most frequent species (number of occurrences), and give reasons when not following this rule in the "comment" column.

light requirement	life form	species	number of occurrences	comment
light-demanding	shrub	***Juniperus communis***	184	
		Prunus spinosa	177	
		Pinus mugo subsp mugo	142	
		Cotoneaster tomentosus	61	
	tree	*Larix decidua*	1216	economically not important
		Betula pendula	669	difficult to distinguish from *B. pubescens*
		Pinus sylvestris	514	
		Populus tremula	181	
		Pinus mugo subsp. uncinata	129	
shade-tolerant	shrub	***Lonicera nigra***	669	
		Vaccinium myrtillus	484	often missed because of 40 cm height threshold
		Lonicera alpigena	286	already one *Lonicera* species selected
		Daphne mezereum	168	
		Daphne laureola	62	
	tree	***Picea abies***	4603	
		Fagus sylvatica	3270	
		Acer pseudoplatanus	2550	
		Abies alba	2392	
		Ulmus glabra	503	
		Carpinus betulus	296	
		Tilia cordata	246	
		Tilia platyphyllos	178	
		Taxus baccata	98	
		Pseudotsuga menziesii	85	

748 **Table A2** A description of the topographic, soil, and climatic predictors that were used by at least one model.

Predictor		Description
topography	c_slope	Average slope of the above catchment based on the multiple flow direction (MFD) algorithm
	slope	Slope (gradient) for each cell based on 3x3 window
	convexity_3	Convexity is calculated as the ratio of the number of cells having positive curvature (= convex cells) to the number of cells within a radius of 3 cells.
	convexity_12	Convexity is calculated as the ratio of the number of cells having positive curvature (= convex cells) to the number of cells within a radius of 12 cells.
	melton_rug	Melton ruggedness index. Ratio of the upslope catchment height and catchment area based on the single flow direction.
	stream_power	A measure of the erosive power of flowing water. SPI is calculated based upon slope and contributing area.[1] Wilson, J.P., 2012. Digital terrain modeling. Geomorphology 137(1), 107-121.
	twi_mfd	Topographic Wetness Index based on the multiple flow direction (MFD) algorithm[2].
	terhet_sd	terrain heterogeneity: standard deviation of a digital elevation model with 5 m resolution
soil	soil_pH	The topsoil pH map was calculated based on 1944 forest soil profiles using the random forest model implementation of the caret R package (v 6.0-68)[3]. We used 80% of the soil profiles as training set, 20% as independent validation set. A total of 126 predictors were used to describe topography, climate and geology. The R2 of the validation set was 0.37, the root mean squared error was 1.08.
climate	bio_4	Temperature Seasonality[4]
	bio_13	Precipitation of Wettest Month[4]
	bio_14	Precipitation of Driest Month[4]
	gdd	growing degree days[4]
	etpt	potential evapotranspiration[4]
	mind	moisture index: difference between precipitation and potential evapotranspiration[4]
	pdsum	number of days with rainfall >1 mm[5]
	prec_suwirat	ratio of summer (April to September) to winter (October to March) precipitation sums[4]
	prec_su	summer precipitation sum (April to September)[4]
	swb	site water balance[5]

tave_suwirat	ratio of average summer (April to September) to average winter (October to March) temperature[4]
tave_wi	average winter (October to March) temperature[4]
tave_su	average summer (April to September) temperature[4]

[1] Colgan, A., & Ludwig, R. (2016). Digital Terrain Model. In *Regional Assessment of Global Change Impacts* (Vol. 137, pp. 69–74). Cham: Springer International Publishing. https://doi.org/10.1007/978-3-319-16751-0_7

[2] Böhner, J., & Selige, T. (2006). Spatial prediction of soil attributes using terrain analysis and climate regionalisation. In J. Böhner, K. R. McCloy, & J. Strobl (Eds.), *SAGA - Analysis and Modelling Applications* (Vol. 115, pp. 13-27.).

[3] Kuhn, M. (2008). Caret package. *Journal of Statistical Software*, 28(5)

[4] Zimmermann, N. E., & Kienast, F. (1999). Predictive mapping of alpine grasslands in Switzerland : Species versus community approach. *Journal of Vegetation Science*, *10*, 469–482.

[5] Guisan, A., Zimmermann, N. E., Elith, J., Graham, C. H., Phillips, S., & Peterson, a. T. (2007). WHAT MATTERS FOR PREDICTING THE OCCURRENCES OF TREES: TECHNIQUES, DATA, OR SPECIES' CHARACTERISTICS? *Ecological Monographs*, *77*(4), 615–630. https://doi.org/10.1890/06-1060.1

Table A3 Results from testing equivalence between subsampled and original point clouds in a test area (2700km^2) with varying point densities. The test area was situated in Central Switzerland (xmin: 700012.5; xmax: 760012.5; ymin: 200012.5; ymax: 245012.5) and consisted of 4.32 million cells (25 m x 25 m). Each sample (in rows) was constructed by randomly subsampling the LiDAR point densities from as high as 15 points/m^2 to the 0.5 points/m^2 minimal density using the "lasthin" routine from the LAStools software (Isenburg, 2015). Using two one sided t-tests (TOST), we checked if the subsampled values were equivalent with the values obtained from the original, mixed-density LiDAR dataset. We considered the results to be equivalent if samples deviated no more than 5% in vegetation cover, 1m in average height, 0.5m in the 5th percentile (p05), 2m in the 95th percentile (p95), and 0.05 in vertical variation (the coefficient of variation). All tests revealed that values from subsampled rasters are equivalent to the values obtained from using the mixed-density LiDAR dataset.

	vegetation cover	**average height**	**p05**	**p95**	**vertical variation**
sample 1	equivalent	equivalent	equivalent	equivalent	equivalent
sample 2	equivalent	equivalent	equivalent	equivalent	equivalent
sample 3	equivalent	equivalent	equivalent	equivalent	equivalent
sample 4	equivalent	equivalent	equivalent	equivalent	equivalent
sample 5	equivalent	equivalent	equivalent	equivalent	equivalent
sample 6	equivalent	equivalent	equivalent	equivalent	equivalent
sample 7	equivalent	equivalent	equivalent	equivalent	equivalent
sample 8	equivalent	equivalent	equivalent	equivalent	equivalent
sample 9	equivalent	equivalent	equivalent	equivalent	equivalent
sample 10	equivalent	equivalent	equivalent	equivalent	equivalent

Table A4 The table lists which predictors (in rows) were included for each of the species (in columns). A value of −1 indicates that the variable was included only in the model without LiDAR predictors, a value of 1 indicates it was only included in the model with LiDAR predictors. Zero indicates the variables was included in both models.

		Daphne mezereum	*Lonicera nigra*	*Fagus sylvatica*	*Picea abies*	*Juniperus communis*	*Prunus spinosa*	*Populus tremula*	*Pinus sylvestris*
climate	bio_13	0	−1		−1			0	
	bio_14		0	−1	0	−1		0	
	bio_4				−1	−1	0		
	gdd			0				−1	0
	etpt	−1					0		
	mind						0		0
	pdsum	0	−1		0	−1	−1	0	−1
	prec_suwirat			−1		0		−1	
	prec_su					0			
	swb		0		−1			−1	
	tave_suwirat			0					
	tave_wi				0				
	tave_wi		0						
soil	soil_pH	0	−1						0
topography	c_slope			0					−1
	convexity_12	−1							
	convexity_3	−1							
	melton_rug								−1
	slope					0			
	stream_power			−1					
	twi_mfd						−1		
	terhet_sd						−1		
LiDAR	average height	1		1	1	1	1	1	1
	vegetation cover	1	1	1	1	1		1	1
	height variation	1	1	1			1		
	foliage height diversity		1		1	1	1	1	1

Table A5 Table that reports on changes in model performance (TSS_{CV}) for each species. The statistics given in each column (min, 25_{th}, 50_{th}, 75_{th} percentile, and max) summarize the results over five models and 20 cross-validation repeats.

light requirement	life form	species	min	25%	50%	75%	max
shade-tolerant	shrubs	*Daphne mezereum*	−48.515	−4.732	6.095	21.678	275.735
		Lonicera nigra	−32.152	−12.377	−7.972	−4.396	8.381
	trees	*Fagus sylvatica*	−15.734	−11.045	−9.074	−7.394	−1.790
		Picea abies	−22.260	−3.679	−0.908	2.872	12.690
light-demanding	shrubs	*Juniperus communis*	−9.830	2.847	13.754	23.367	56.564
		Prunus spinosa	−16.845	−0.830	4.413	9.494	33.682
	trees	*Populus tremula*	−43.708	4.639	23.256	51.580	501.942
		Pinus sylvestris	−10.100	0.082	2.815	7.263	17.674

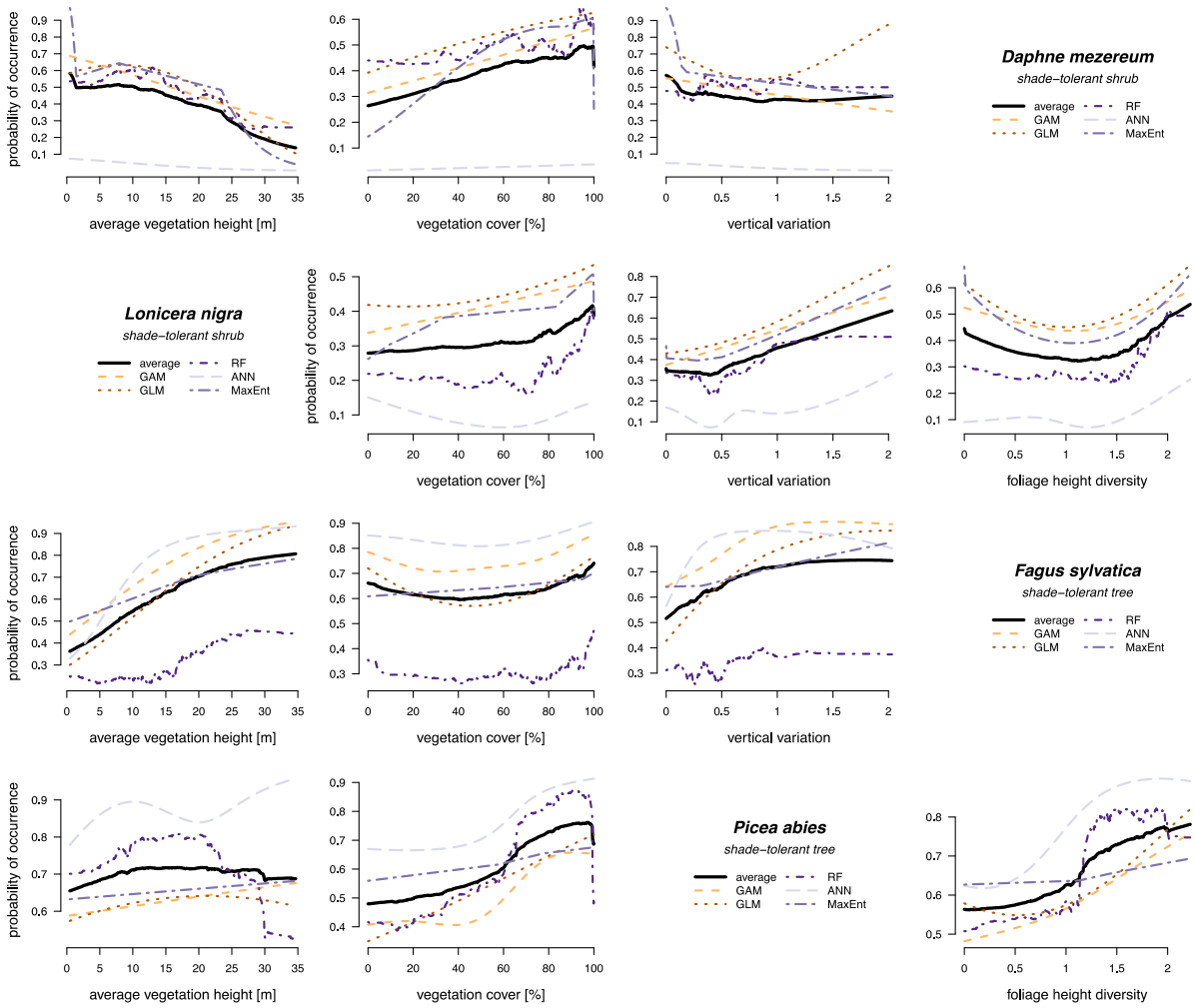

788

789 **Figure A1** Partial response curves for shade-tolerant species (one per row, see legend), with the ensemble
790 probability as black solid line, and the single model predictions with line shapes and colors according to the
791 legend.

792

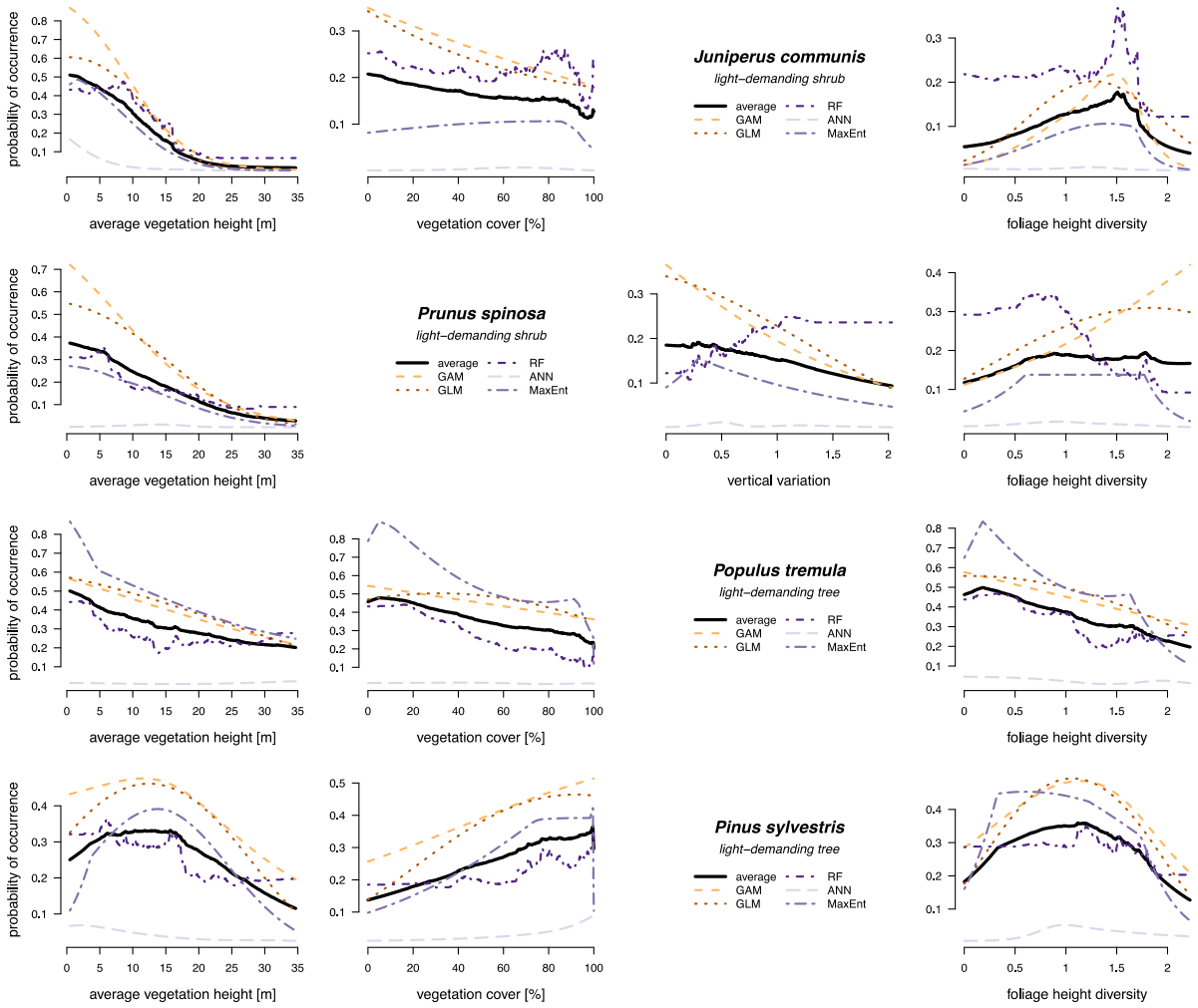

793

794 **Figure A2** Partial response curves for light-demanding species (one per row, see legend), with the ensemble
795 probability as black solid line, and the single model predictions with line shapes and colors according to the
796 legend.